AD-755 104

DEVELOPMENT OF AN E-FRAME FLUIDIC TRANSDUCER

H. Steven Kimmel

Harry Diamond Laboratories
Washington, D. C.

December 1972

UNCLASSIFIED
Security Classification

DOCUMENT CONTROL DATA - R & D

(Security classification of title, body of abstract and indexing annotation must be entered when the overall report is classified)

1. ORIGINATING ACTIVITY (Corporate author) Harry Diamond Laboratories Washington, D.C. 20438	2a. REPORT SECURITY CLASSIFICATION unclassified 2b. GROUP

3. REPORT TITLE

DEVELOPMENT OF AN E-FRAME FLUIDIC TRANSDUCER

4. DESCRIPTIVE NOTES (Type of report and inclusive dates)

5. AUTHOR(S) (First name, middle initial, last name)

H. Steven Kimmel

6. REPORT DATE December 1972	7a. TOTAL NO. OF PAGES ~~24~~ 21	7b. NO. OF REFS 3
8a. CONTRACT OR GRANT NO. b. PROJECT NO. DA-1W262301A30000 cAMCMS Code: 632301.11.62400 dHDL Proj: A20334	9a. ORIGINATOR'S REPORT NUMBER(S) HDL-TM-72-28 9b. OTHER REPORT NO(S) (Any other numbers that may be assigned this report)	

10. DISTRIBUTION STATEMENT

Approved for public release; distribution unlimited.

11. SUPPLEMENTARY NOTES	12. SPONSORING MILITARY ACTIVITY MUCOM

13. ABSTRACT

A theoretical analysis has been conducted by these laboratories to develop a new transducer for use with fluidic generators. Evolving from this study is an E-frame generator that employs an improved magnetic circuit. This circuit consists of an E-shaped reed whose center member vibrates inside a stationary coil. Unlike previous models of the fluidic generator, the reed-coil assembly is positioned outside the magnet-pole piece assembly to reduce eddy current losses. The new design is capable of providing 0.180 W at 210 fps and 2.2 W at 1000 fps.

This report describes the analysis made and evaluates the design parameters investigated during the study.

DD FORM 1 NOV 68 1473 REPLACES DD FORM 1473, 1 JAN 64, WHICH IS OBSOLETE FOR ARMY USE.

I

UNCLASSIFIED
Security Classification

14 KEY WORDS	LINK A		LINK B		LINK C	
	ROLE	WT	ROLE	WT	ROLE	WT
Transducer	8	3				
Power supply	8	3				
Environmental sensor	8	3				

AD

DA-1W262301A30000
AMCMS Code: 632301.11.62400
HDL Proj: A20334

HDL-TM-72-28

DEVELOPMENT OF AN E-FRAME FLUIDIC TRANSDUCER

by

H. Steven Kimmel

December 1972

US ARMY MATERIEL COMMAND
HARRY DIAMOND LABORATORIES
WASHINGTON, DC 20438

FOREWORD

The analysis presented in this report was conducted for USA Munitions Command under the Components, Materials, and Techniques (CMT) Program, Department of Army Project 1W262301A30000. The work reported covers the period of March to July 1972 and completes the objectives of this project.

The author gratefully acknowledges the contributions made toward this investigation by staff member, Dr. Carl J. Campagnuolo.

CONTENTS

FIGURES

1. INTRODUCTION

This report discusses a fluidic generator that uses a new magnetic configuration to convert mechanical motion into electrical energy. Previous models of the fluidic generator have surrounded the coil with the pole pieces.[1] Figure 1 is a schematic representation of previous fluidic generator models. The adaptation of this new magnetic circuit to the fluidic generator is shown in figure 2. The new circuit consists of an E-shaped reed whose center member vibrates inside a stationary coil. The reed-coil assembly is positioned outside the magnet-pole piece assembly to improve the design efficiency.

A theoretical discussion is presented, as well as an evaluation of the parameters studied.

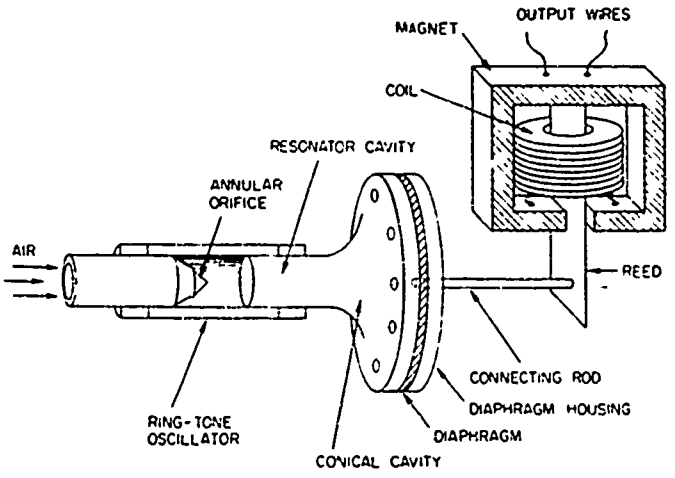

Figure 1. Schematic diagram of fluidic generator with ringtone oscillator.

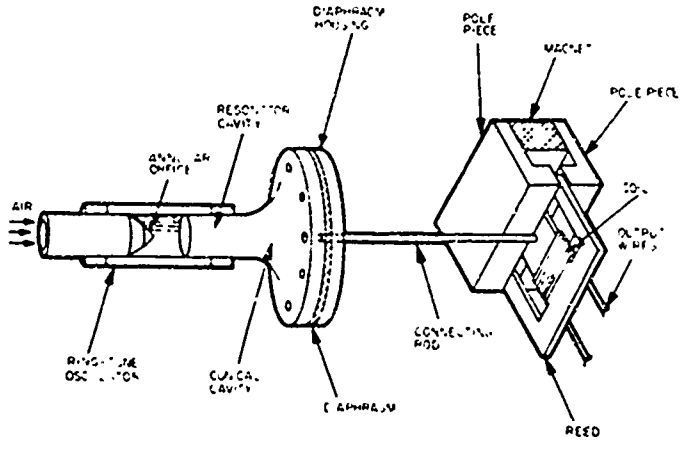

Figure 2. Schematic diagram of fluidic generator with new E-frame transducer.

[1] Kimmel, H.S., "Development of a Fluidic Velocity Sensor," March 1974, Harry Diamond Laboratories, Washington, D.C., HDL-TM-72-6.

2. DESIGN AND OPERATION OF E-FRAME GENERATOR

2.1 Design Description

Figure 2 is a schematic diagram of an E-frame generator that operates when air passes through an annular orifice into a resonating cavity. The resonating cavity is connected to a conical cavity and is sealed by a metal diaphragm. The aligned orifice and closed cavity form a ring-tone oscillator[2] that produces acoustical oscillations of the incoming air. These acoustical vibrations trigger the diaphragm into a mechanical resonance. A connecting rod imparts the motion of the diaphragm to the E-frame reed placed in the airgap of the new magnetic circuit. Two flux paths are generated as the center member of this reed is driven between the poles of the magnetic circuit. Each flux path follows the outer reed member and passes through the pole piece before returning to the center reed member. The changing of the flux fields in the center member of the E frame generates the voltage in the stationary coil.

2.2 Description of Magnetic Circuit

The principal differences between the earlier magnetic circuit and the new magnetic circuit are shown in figure 3. The earlier circuit has a coil contained within the pole-piece structure. The vibratory motion of the reed generates a differential flux through the reed and pole pieces as shown by the dashed arrows. This transducer has two disadvantages.[3] First, the ac flux component travels the length of the pole pieces, which are highly biased by a dc flux component. Secondly, the pole pieces surround the coil volume, resulting in a substantial amount of flux leakage.

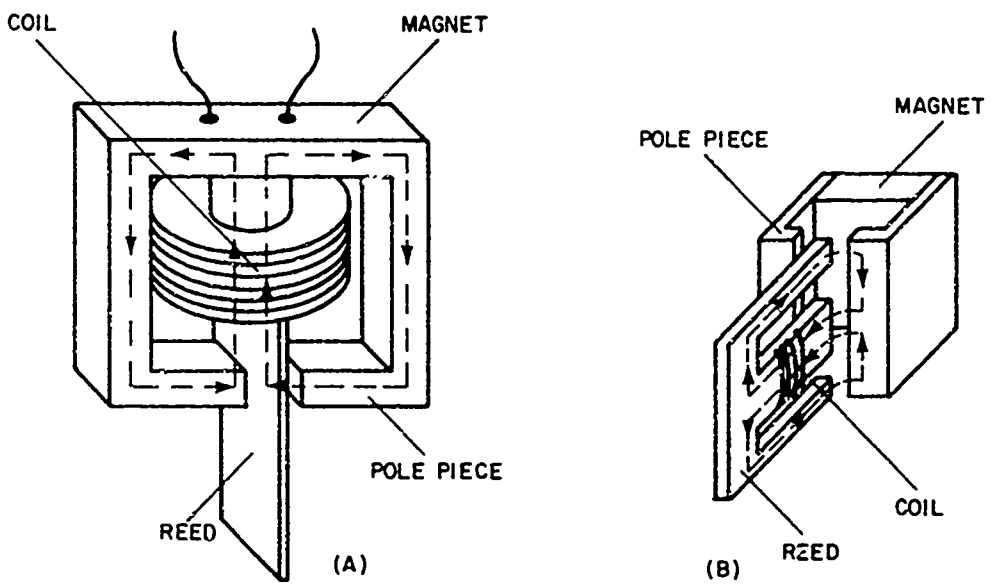

Figure 3. Comparison of (a) original and (b) new E-frame magnetic transducers.

---

[2] Campagnuolo, C.J. and Lee, H., "Review of Some Fluid Oscillators," April 1969, Harry Diamond Laboratories, Washington, D.C., HDL-TR-1438.

[3] Bauer, B.B., "A Miniature Microphone for Transistorized Amplifiers," Journal of Acoustical Society of America, Vol. 25, pp. 867-869, Sept 1953.

In the new design, the coil is moved outside the magnetic structure and positioned to allow the center member of the reed to vibrate through its center. Each side of the coil is bordered by a relatively stationary member of the reed. This change shortens the a-c flux path in the pole pieces (as shown by the dashed arrows in fig. 3) by decoupling the a-c and d-c flux fields. The flux path length is essentially the same; however, the a-c flux is only superimposed upon the d-c flux through the relatively short pole-piece region. Furthermore, this design provides two substantially separate magnetic circuits that are summed in the center airgap and are otherwise complete in themselves.[3]

3. THEORETICAL CONSIDERATIONS

Bauer (ref 3) analyzed the magnetic circuit shown in figure 4. His analysis began with the amount of surface area of the center member of the reed, A_R, that is moved to the right a distance X. The total flux (ϕ_1) in this vibrating member was determined to be

$$\phi_1 = \frac{F_g X}{2R_o L_g} \quad , \tag{1}$$

where F_g = magnetomotive force present in the airgap

X = distance displaced to the right

R_o = reluctance of the outside airgap

L_g = airgap length

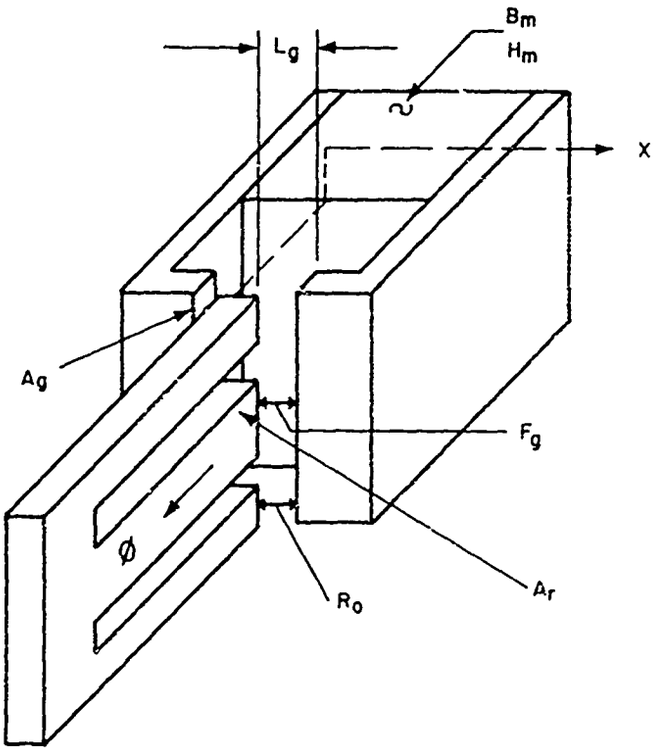

Figure 4. Schematic diagram showing parameters of the E-frame magnetic circuit.

The motion of the center reed member generates a voltage (e) in a coil of n turns proportional to ϕ_1 as given by

$$e = 10^{-8} \frac{d_{\phi_1}}{d\tau} \text{ volts}, \tag{2}$$

where τ is time in seconds.

Combining equations 1 and 2 yields

$$e = \frac{10^{-8} n F_g}{2R_o L_g} \frac{dx}{d\tau} \text{ volts}. \tag{3}$$

Equation 3 shows the proportionality between the parameters of the magnetic circuit and the availability of output voltage. This proportionality may be viewed as the dynamic responsiveness of the magnetic circuit. The static potential of this magnetic circuit was analyzed by Parker and Studders.[4] They made an analysis of a similar magnetic arrangement and derived an expression for the leakage factor F_1. The leakage factor is the ratio of total flux in the magnet to the flux in the airgap and is expressed by the following quantities:

$$F_1 = \frac{V_m B_m H_m}{L_g H_g^2 A_g} , \tag{4}$$

where V_m = magnet volume

B_m = magnetic induction of the magnet

H_m = magnetic potential of the magnet

H_g = magnetic potential of the airgap

A_g = surface area of the reed in the airgap

L_g = airgap distance

Thus, the magnetic circuit must possess some optimum amount of internal energy that can be delivered efficiently to the airgap or working medium. For maximum energy transfer, F_1 should approach unity. Equations 3 and 4 fully describe the parameters investigated in this study.

4. EXPERIMENTAL ANALYSIS

4.1 Approach

This study began by improving the amount of magnet potential ($V_m B_m H_m$) within the confines of space, weight, and size considerations. The reduction of F_1 is then achieved by increasing the energy potential

---

[4] Parker, R.J. and Studders, R.J., Permanent Magnets and Their Application, John Wiley and Sons, N.W., 1967.

in the airgap ($L_g H_g^2 A_g$). An increase in L_g reduces H_g so that a compromise solution must be obtained. Meanwhile equation 3 suggests that L_g must be decreased to increase the output voltage. Physical restrictions are placed on the lower limit of L_g, since the reed's thickness and total displacement must be less than L_g. A parametric study was begun using equations 3 and 4 as a guide with physical considerations as constraints.

4.2 Results of the Parametric Study

The components of the E-frame generator are shown in figure 5. A test setup with experimental apparatus used for the parameter study is block diagrammed in figure 6. The selection of Alnico 5 as the material for the permanent magnet optimized the product $H_m B_m$ of the total flux potential of the magnet ($H_m B_m V_m$ of equation 4). Alnico 5 has one of the highest energy products per pound ($H_m B_m / V_m$) of any of the Alnico magnet family. The selection of this material required only the variation of the magnet volume, V_m, to maximize the internal energy potential of the magnet.

A E-frame generator was assembled with unannealed soft iron pole pieces and 4 cm^3 of Alnico 5 magnet material. (This initial volume was selected because previous fluidic generators used this amount. The upper limit of the magnet volume was defined by the space considerations of height and diameter of the transducer.) Figure 7 shows that the available output power at 1 psig was increased from 125 to 200 mW with an increase of V_m from 4 to 6 cm^3. The percentage increase of output power decreased over the operating range from 1 to 10 psig and was attributed to eddy-current losses in the pole-piece armature. Since eddy-current losses are primarily a function of the electrical resistivity of the pole piece, different pole-piece materials were investigated; and by heat treating each of these different pole pieces to eliminate cold worked stresses, improved magnetic properties could be achieved. The materials for this study included soft iron and 49-percent nickel steel. The electrical resistivity of soft iron is 10 μΩ/cm, whereas 49-percent nickel steel is 45 μΩ/cm. Figure 8 shows the results of these pole-piece materials with 6 cm^3 of magnet material. As shown, the annealed 49-percent nickel steel produced 0.270 W at 1 psig and 1.375 W at 8 psig.

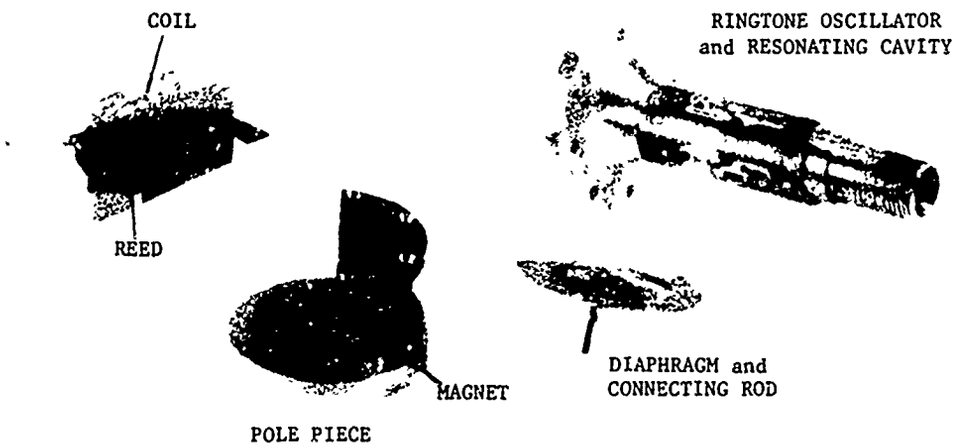

Figure 5. Components of E-frame fluidic generator.

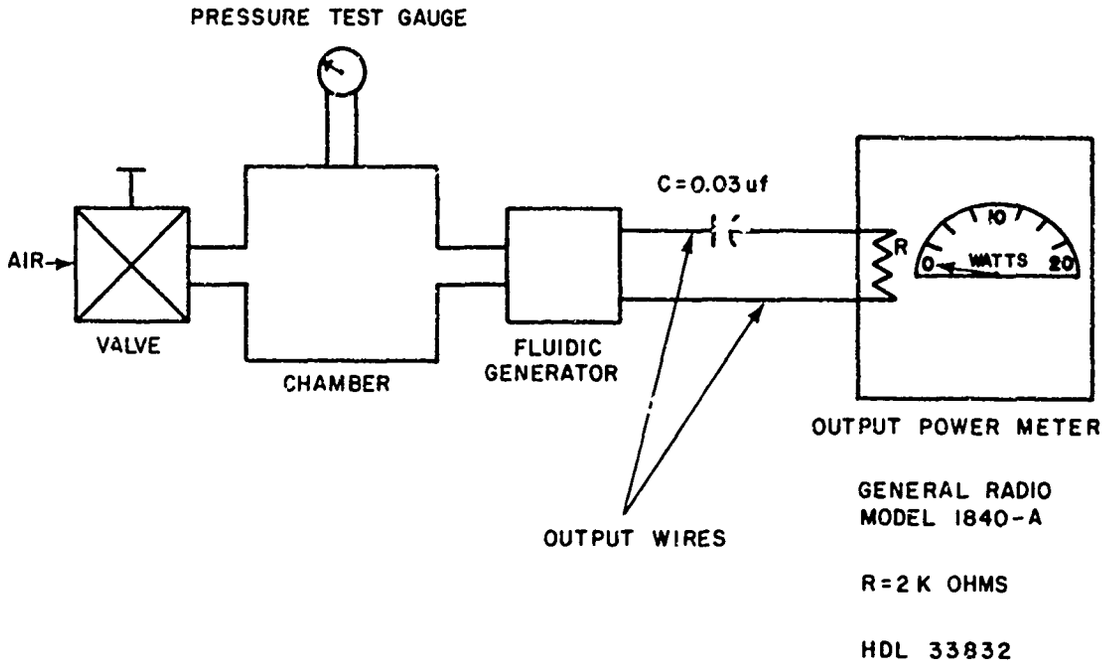

Figure 6. Laboratory arrangement of calibrated test equipment.

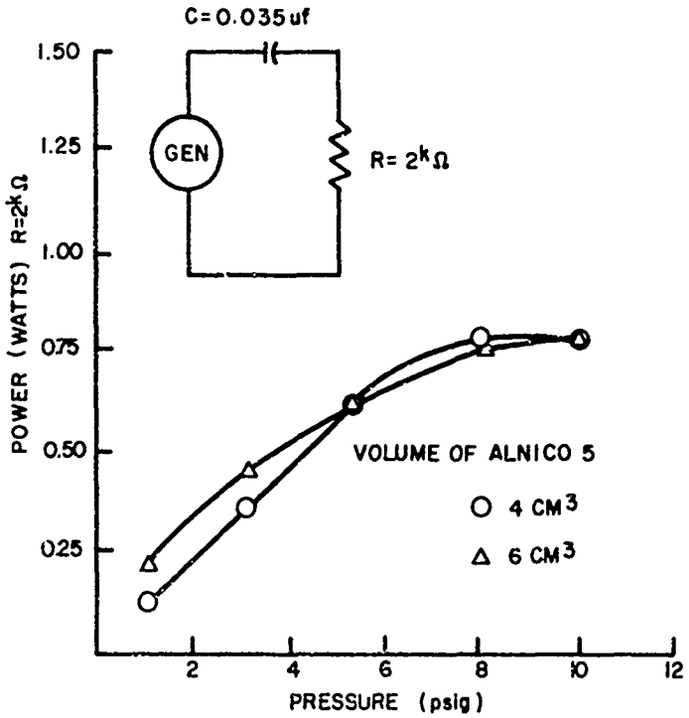

Figure 7. Effects of magnet volume upon output power.

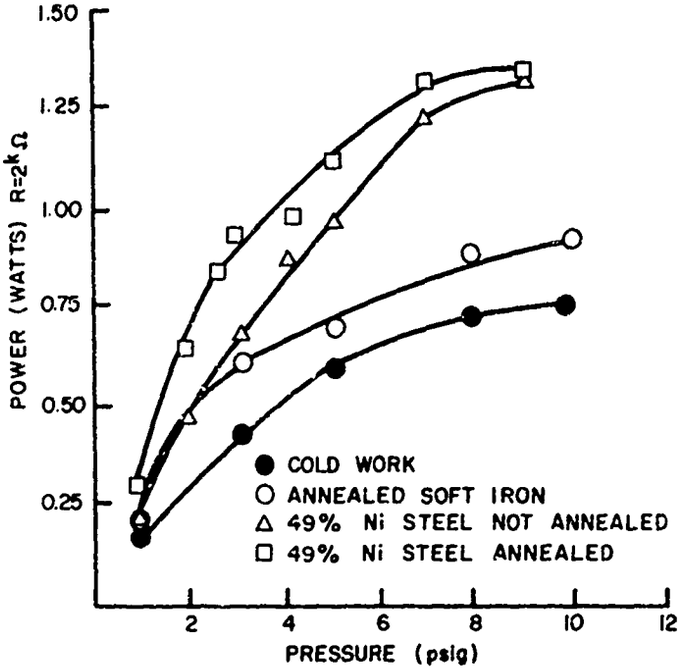

Figure 8. Effects of pole piece material upon output power.

Figure 9 shows the effects of varying the magnetic flux in the vibrating reed (ϕ_1). This parameter change was accomplished by decreasing the intrusion of the outside reed into the constant cross-section airgap (A_g), along with an increase in the width of the airgap (L_g). The original configuration had 0.045 in. airgap with all members of the reed intruding a distance of 0.115 in. into this airgap. As the outer members of the reed were shortened (0.200 in.) so that they became a maximum distance of 0.085 in. away from the pole piece, the output increased only slightly. The greatest increase occurred when the airgap was increased to 0.055 in. The combination of locating the outer members a distance of 0.085 in. away from the pole piece and the inner member a distance of 0.115 in. into this 0.055 in. airgap produced 0.275 W at 1 psig and 1.75 W at 9 psig.

Equation 3 suggests that the reduction in the reluctance (R_o) of the airgap increases the output voltage. Reluctance is dependent upon the cross-sectional area of the airgap and the amount of surface area of intrusion of the reed, A_R. Figure 10 shows the results of varying the intrusion of the reed into the airgap. The airgap length for these tests was held constant at 0.055 in. and the cross-sectional area of the airgap, A_g, was held constant at 0.075 in^2. As the center reed member was reduced from a length of 0.230 to 0.180 in. (so that the amount of intrusion was 0.180 - 0.115 = 0.065 in.)

$$A_R = \text{width of reed member} \times \text{intrusion into airgap}$$
$$= 0.300 \times 0.065 = 0.195 \text{ in.}^2,$$

the output power increased. Next, the outside E-frame members were lengthened an additional 0.010 in. until they became 0.065 in. away from the airgap. The net effect of varying the E-frame members is shown in figure 10, where the output power was increased to 0.4 W at 1 psig and 2.0 W at 8 psig.

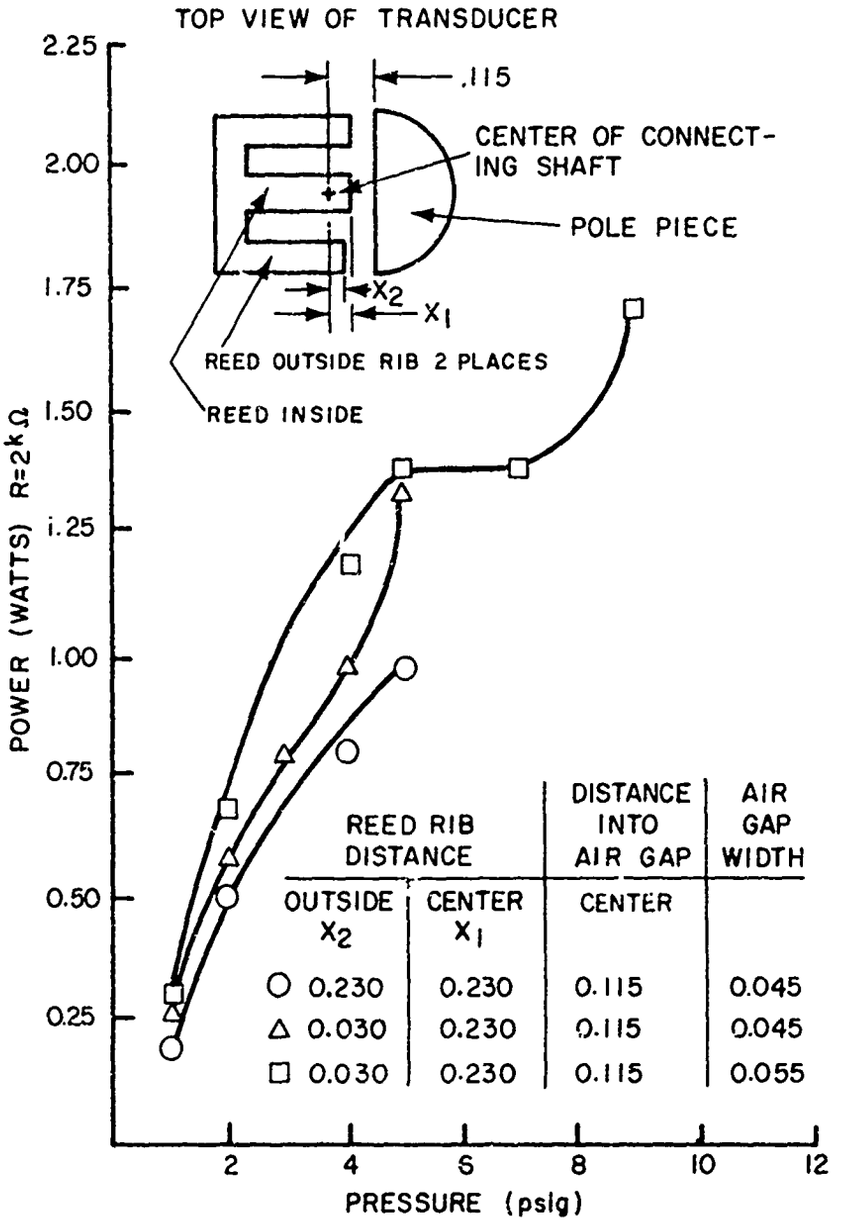

Figure 9. Effects of airgap size and reed location versus output power.

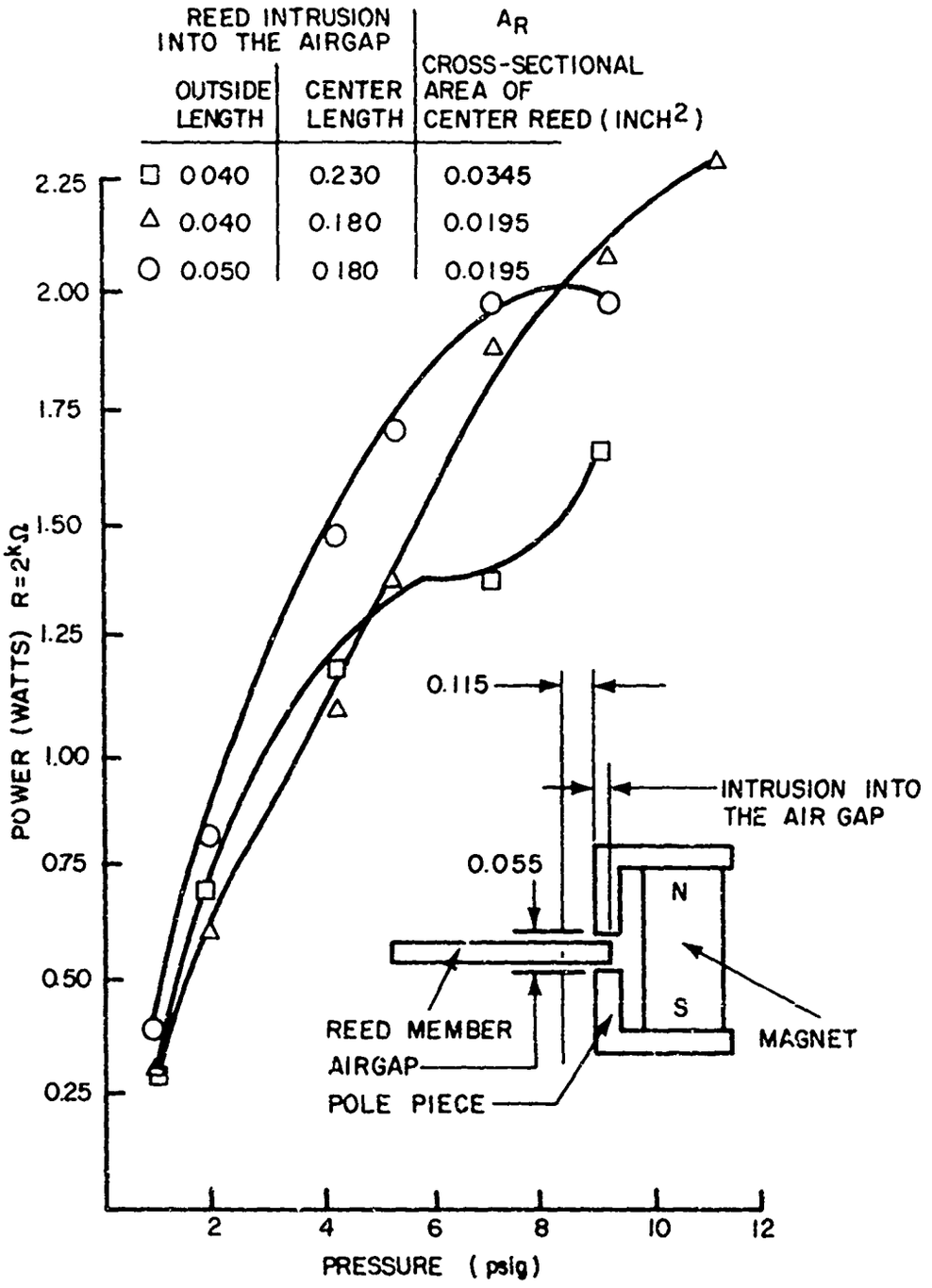

Figure 10. Effects of reed member location versus output power.

Figure 11 shows the results of increasing the airgap in the vicinity of the center- and outer-reed members. Initially, the airgap was uniform at 0.055 in. The airgap was increased to 0.065 in., increasing L_g and thus resulting in a decrease of output power. The center airgap was returned to 0.055 in., and the outside airgaps were increased to 0.075 in. The increased outside airgaps further reduced the reluctance (R_o) and increased the amount of magnetomotive force within the center airgap. Other airgap combinations were investigated, but those with 0.075-in. outside and 0.055-in. inside airgaps provided the largest output power of 0.5 W at 1 psig and increased to a respectable 1.35 W at 9 psig as shown in figure 11.

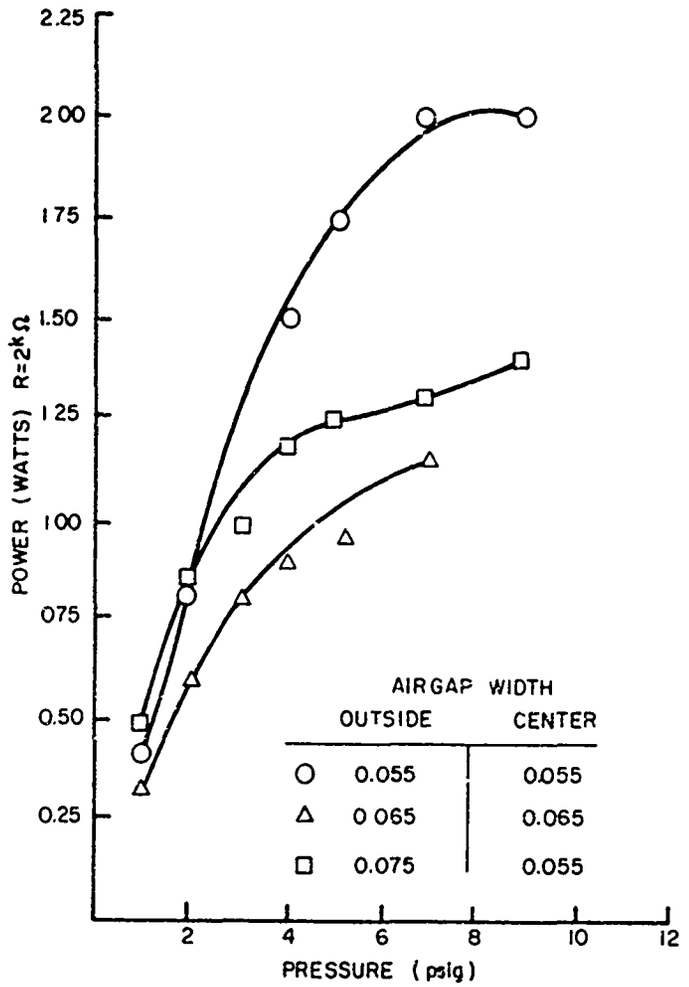

Figure 11. Effects of airgap sizes versus output power.

The last parameter studied was the location of the coil. From equation 3, the amount of available voltage is proportional to dx/dt. Figure 12 shows the results of varying the position of the coil. The maximum output is achieved when the coil is placed closest to the pole pieces. This allows the maximum displacement of the vibrating center-reed member within the coil. The method of attaching the connecting rod to the center of the reed prevented the movement of the face of the coil to a distance less than 0.085 in. from the center line of the connecting rod. However, the positioning of the coil combined with the other parameter changes resulted in an energy transformation of 0.575 W at 1 psig and 2.2 W after 8 psig.

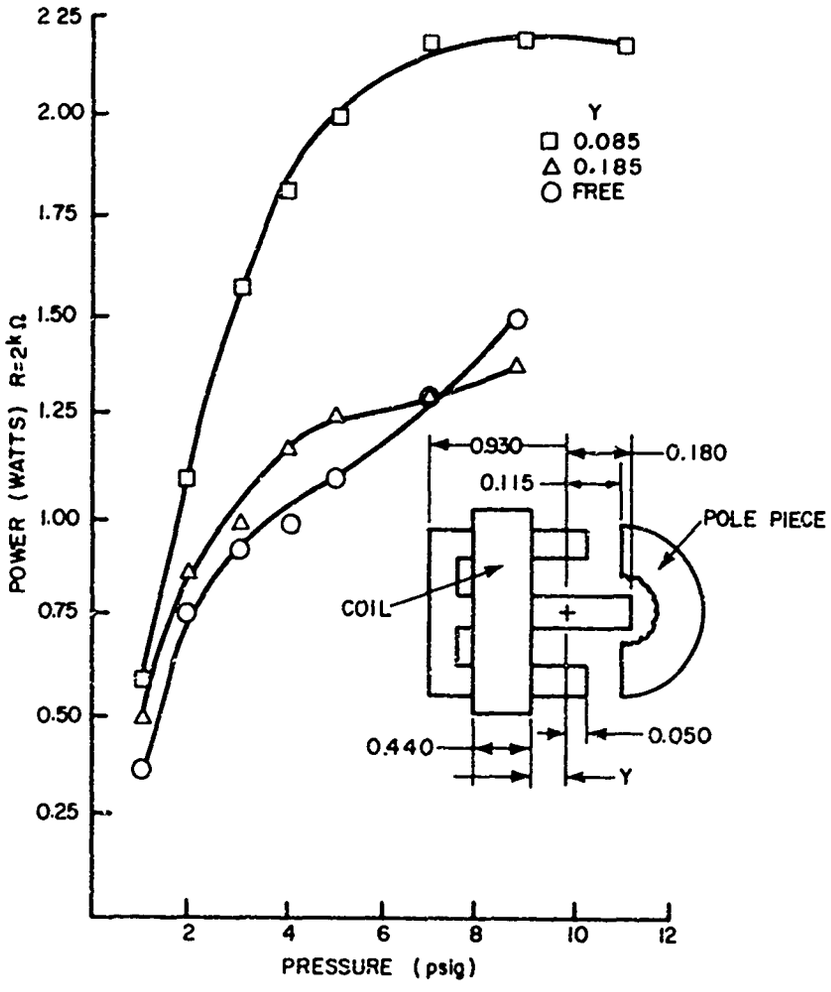

Figure 12. Effects of coil position versus output power.

5. SUMMARY

A parametric investigation has been conducted to develop a new magnetic transducer for the fluidic generator. The investigation was guided by the design equations analyzing the magnetic circuit. Although only a preliminary analysis was performed, the resultant fluidic generator shown in figure 13 produced more power than a single conventional transducer. Converting pressures to velocity (fps) at sea level provides an indication of the usefulness of this new E-frame fluidic generator. As shown in figure 14, the design is capable of providing 0.180 W at 210 fps and 2.2 W at 1000 fps.

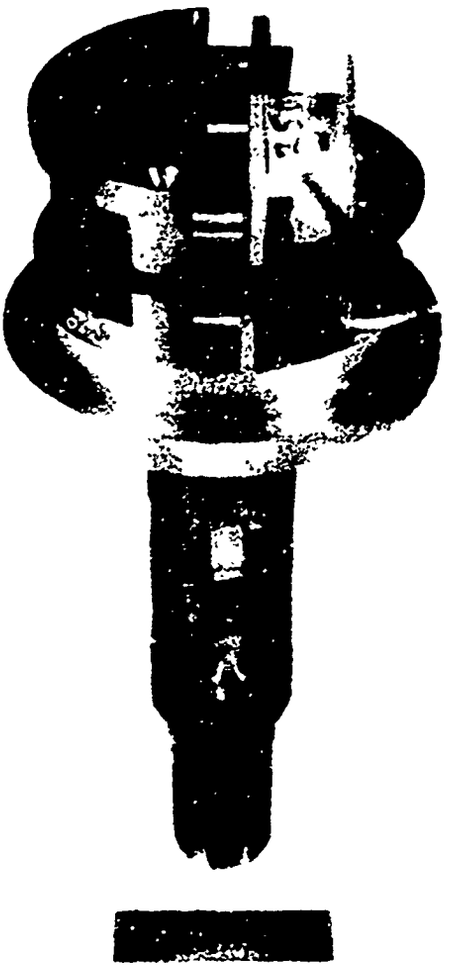

Figure 13. An assembled fluidic generator modified with an E-frame transducer.

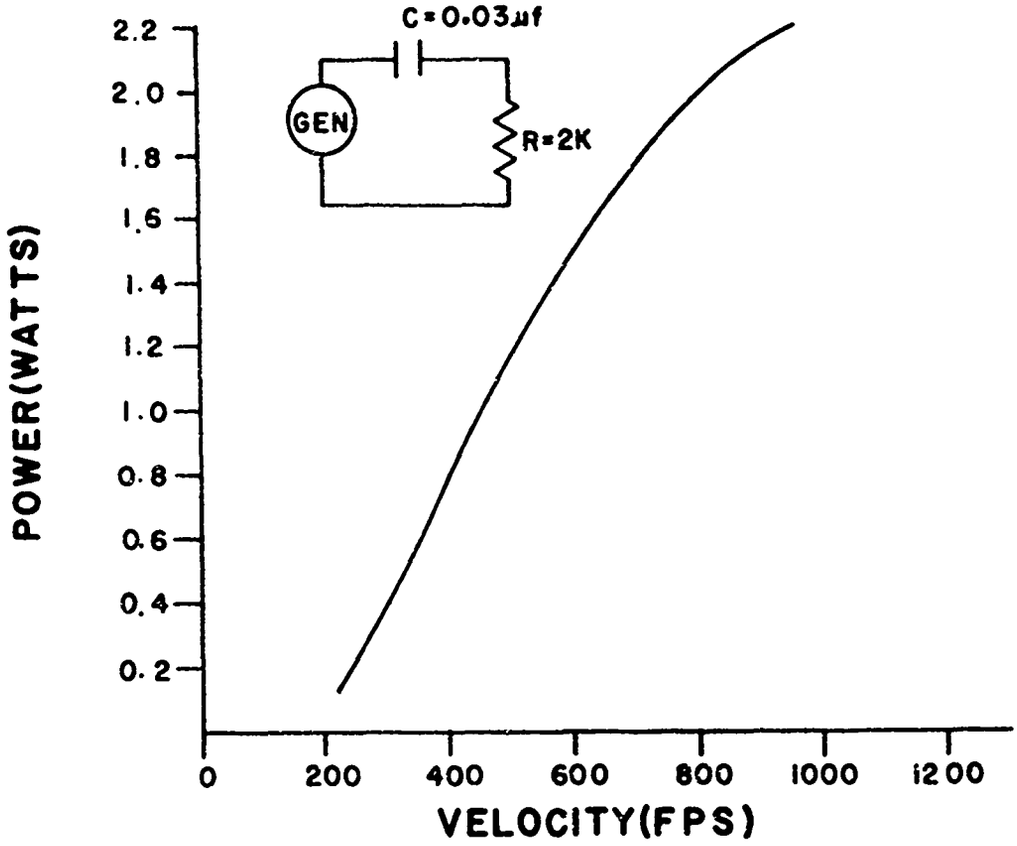

Figure 14. Electrical output of E-frame fluidic generator.